Available online at www.sciencedirect.com
ScienceDirect
Ceramics International 37 (2011) 1353–1357
CERAMICS INTERNATIONAL
www.elsevier.com/locate/ceramint

Mechanical synthesis and rapid consolidation of a nanocrystalline $5.33Fe_{0.37}Cr_{0.16}Al_{0.4}Si_{0.07}$–$Al_2O_3$ composite by high-frequency induction heating

In-Jin Shon [a,b,*], Song-Lee Du [a], In-Yong Ko [a], Tae-Wan Kim [a], Jung-Mann Doh [c], Jin-Kook Yoon [c], Sang-Whan Park [c]

[a] Division of Advanced Materials Engineering and Research Center of Advanced Materials Development, Engineering College, Chonbuk National University, Chonbuk, 561-756, Republic of Korea
[b] Department of Hydrogen and Fuel Cells Engineering, Specialized Graduate School, Chonbuk National University, Chonbuk, 561-756, Republic of Korea
[c] Advanced Functional Materials Research Center, Korea Institute of Science and Technology, P.O. Box 131, Cheongryang, Seoul 130-650, Republic of Korea

Received 11 October 2010; received in revised form 15 November 2010; accepted 15 December 2010
Available online 21 January 2011

Abstract

Nanopowders of $5.33Fe_{0.37}Cr_{0.16}Al_{0.4}Si_{0.07}$ and Al_2O_3 were synthesized from Fe_2O_3, Cr, Si, and Al powders by high-energy ball milling. A high-density nanocrystalline $5.33Fe_{0.37}Cr_{0.16}Al_{0.4}Si_{0.07}$–$Al_2O_3$ composite was consolidated by a high-frequency, induction-heated sintering (HFIHS) method within three minutes from mechanically synthesized powders of Al_2O_3 and $5.33Fe_{0.37}Cr_{0.16}Al_{0.4}Si_{0.07}$. The advantage of this process is that it allows very quick densification to near theoretical density and prohibits grain growth in nano-structured materials. The average grain sizes of Al_2O_3 and $5.33Fe_{0.37}Cr_{0.16}Al_{0.4}Si_{0.07}$ were 99 nm and 14 nm, respectively.

Keywords: Nanostructured materials; A. Sintering; Mechanical alloying; C. Mechanical properties; Composite materials

1. Introduction

Many industrial applications, such as heating elements, high-tensile components in heat exchangers, or substrates for catalysts applied in catalytic converter and filter systems in automobiles require long-term resistance to oxidation. Iron–aluminium–chromium alloys are applicable as structural materials and coatings for high-temperature applications [1]. Their excellent corrosion resistance is due to the formation of a dense, protective alumina scale. Alumina (α–Al_2O_3 in particular) demonstrates a low rate constant, even at temperatures above 1000 °C [2]. The effects of adding silicon on the high-temperature oxidation resistance and microwave properties of steels have been presented by several authors [3,4]. They suggest that silicon has a beneficial effect on the oxidation resistance and microwave properties of steel. However, the alloy exhibits a low frictional resistance due to its low hardness. One method to improve hardness is adding Al_2O_3 to form composite nanostructured materials [5]. Traditionally, discontinuously reinforced metal matrix composites have been produced by several processes, including powder metallurgy, spray deposition, mechanical alloying, casting, and self-propagating high-temperature synthesis (SHS). A technique that uses high-energy ball milling and mechanical alloying of powder mixtures (which is a combination of mechanical milling and chemical reactions) has been reported as an efficient method for preparing nanocrystalline metals and alloys [6].

Nanocrystalline materials have received much attention as advanced engineering materials, due to their improved physical and mechanical properties [7,8]. Nanomaterials typically possess high strength, high hardness, excellent ductility, and toughness. Therefore, increasing attention has been paid to developing potential nanomaterial applications [9]. The grain

* Corresponding author at: Division of Advanced Materials Engineering and Research Center of Advanced Materials Development, Engineering College, Chonbuk National University, Chonbuk, 561-756, Republic of Korea.
Tel.: +82 63 2381; fax: +82 63 270 2386.
E-mail address: ijshon@chonbuk.ac.kr (I.-J. Shon).

0272-8842/$36.00
doi:10.1016/j.ceramint.2010.12.008

sizes are much larger in sintered materials than in pre-sintered powders, due to the fast grain growth that occurs during the conventional sintering processes. Therefore, even though the initial particle size is less than 100 nm, the grain size increases rapidly up to 2 μm or larger during the conventional sintering [10]. So, controlling grain growth during sintering is one of the keys to the commercial success of nanostructured materials. High-frequency, induction-activated sintering methods, which can be used to quickly manufacture dense materials within 2 min, can control grain growth effectively [11,12].

The goals of this work were to fabricate a new nanopowder using high-energy ball milling and a dense nanocrystalline Al_2O_3-reinforced Fe–Cr–Al–Si composite within three minutes from mechanically alloyed powders via a high-frequency, induction-activated sintering method and to evaluate its hardness and grain size.

2. Experimental procedures

Powders of 99% pure Fe_2O_3 (<5 μm, Alfa Co.), 99.5% pure Al (<325 mesh, Alfa Co.), 99.5% pure Si (<325 mesh, Alfa Co.), and 99.8% pure Cr (<10 μm, Alfa Co.) were used as the starting materials. Fe_2O_3, 0.85 Cr, 0.4 Si, and 4.07 Al powder mixtures were milled in a high-energy ball mill (Pulverisette 5 planetary mill) at 250 rpm for 10 h to produce Al_2O_3 + 5.33-$Fe_{0.37}Cr_{0.16}Al_{0.4}Si_{0.07}$. Tungsten carbide balls (8.5 mm in diameter) were used in a sealed cylindrical stainless steel vial under an argon atmosphere. The weight ratio of the balls to the powder was 30:1. Milling resulted in a significant reduction of grain size. The grain sizes of the Fe–Cr–Al–Si alloy and Al_2O_3 were calculated using Suryanarayana's and Norton's formula [13]:

$$B_r(B_{\text{crystalline}} + B_{\text{strain}})\cos\ \theta = k\frac{\lambda}{L} + \sin\ \theta \quad (1)$$

where B_r is the full width at half-maximum (FWHM) of the diffraction peak after instrument correction, $B_{\text{crystalline}}$ and B_{strain} are the FWHM values caused by the small grain size and internal stress, respectively, k is a constant with a value of 0.9, λ is the wavelength of the X-ray radiation, L is the grain size, η is the internal strain, and θ is the Bragg angle. The parameters B and B_r follow Cauchy's form with the relationship $B = B_r + B_s$, where B and B_s are the FWHM values of the broadened Bragg peaks and the standard sample's Bragg peaks, respectively.

After milling, the mixed powders were placed in a graphite die (outside diameter of 45 mm, inside diameter of 20 mm, height of 40 mm) and then introduced into an induced current activated sintering system (Eltek, South Korea), which is shown schematically in [11]. The four major stages in the synthesis are: stage (1) evacuation of the system, stage (2) application of uniaxial pressure, stage (3) heating of the sample by an induced current, and stage (4) cooling of the sample. The process was conducted under a vacuum of 40 mTorr.

Microstructural information was obtained from product samples that were polished at room temperature. Compositional and microstructural analyses of the products were conducted using X-ray diffraction (XRD) and a scanning electron microscope (SEM) with energy dispersive X-ray analysis (EDAX). The Vickers hardness was measured by performing indentations on the sintered samples at a load of 10 kg and a dwell time of 15 s.

3. Results and discussion

The X-ray diffraction results for the high-energy, ball-milled powders are shown in Fig. 1. The Fe_2O_3, Cr, Si, and Al reactant powders were not detected, while the Fe–Cr–Al–Si alloy and Al_2O_3 were detected. Based on the above results, the mechanical alloy was completely formed during the milling. The net reaction can be considered as a combination of the following two reactions.

$$Fe_2O_3 + 2Al \rightarrow 2Fe + Al_2O_3 \quad (2)$$

$$2Fe + 0.85Cr + 2.07Al + 0.4Si \rightarrow 5.33Fe_{0.37}Cr_{0.16}Al_{0.4}Si_{0.07} \quad (3)$$

Reaction (2) is the well known exothermic reaction for which the standard enthalpy of reaction ranges from −847 kJ to −811 kJ over the temperature range of 700 °C (just above the melting temperature of Al, 660 °C) to 1500 °C (just below the melting point of Fe, 1536 °C).

Fig. 2 shows an FE-SEM image and X-ray mapping (O, Al, Si, Fe, and Cr) of high-energy, ball-milled powders. The powders are very fine and agglomerated. In X-ray mapping, O and Al are detected in the same position, and Fe, Cr, Al, and Si are also in the same position. Therefore, mechanical alloying during the milling can be conformed. The particle size cannot be calculated by the linear intercept method, due to the agglomeration of powders. Fig. 3 shows a plot of $B_r \sin\theta$ as a function of $\cos\theta$ to calculate particle size using Suryanarayana's and Norton's formula [13]. The intercept ($K\lambda/L$) can be

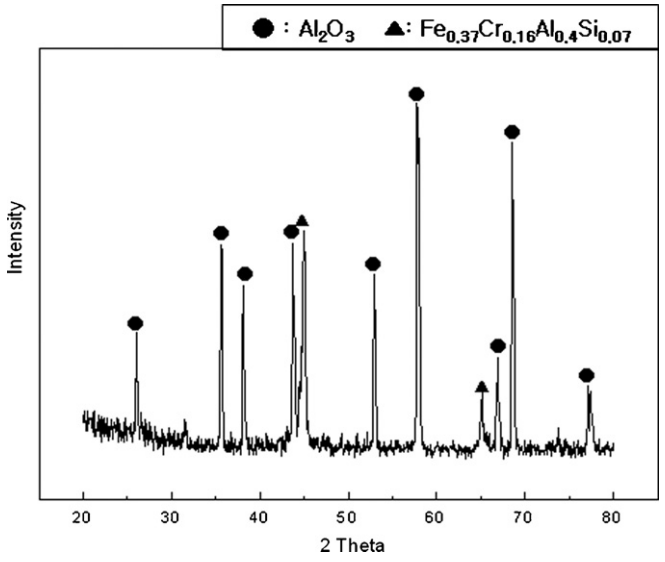

Fig. 1. XRD pattern of the mechanically alloyed $5.33Fe_{0.37}Cr_{0.16}Al_{0.4}Si_{0.07}$–$Al_2O_3$ powder.

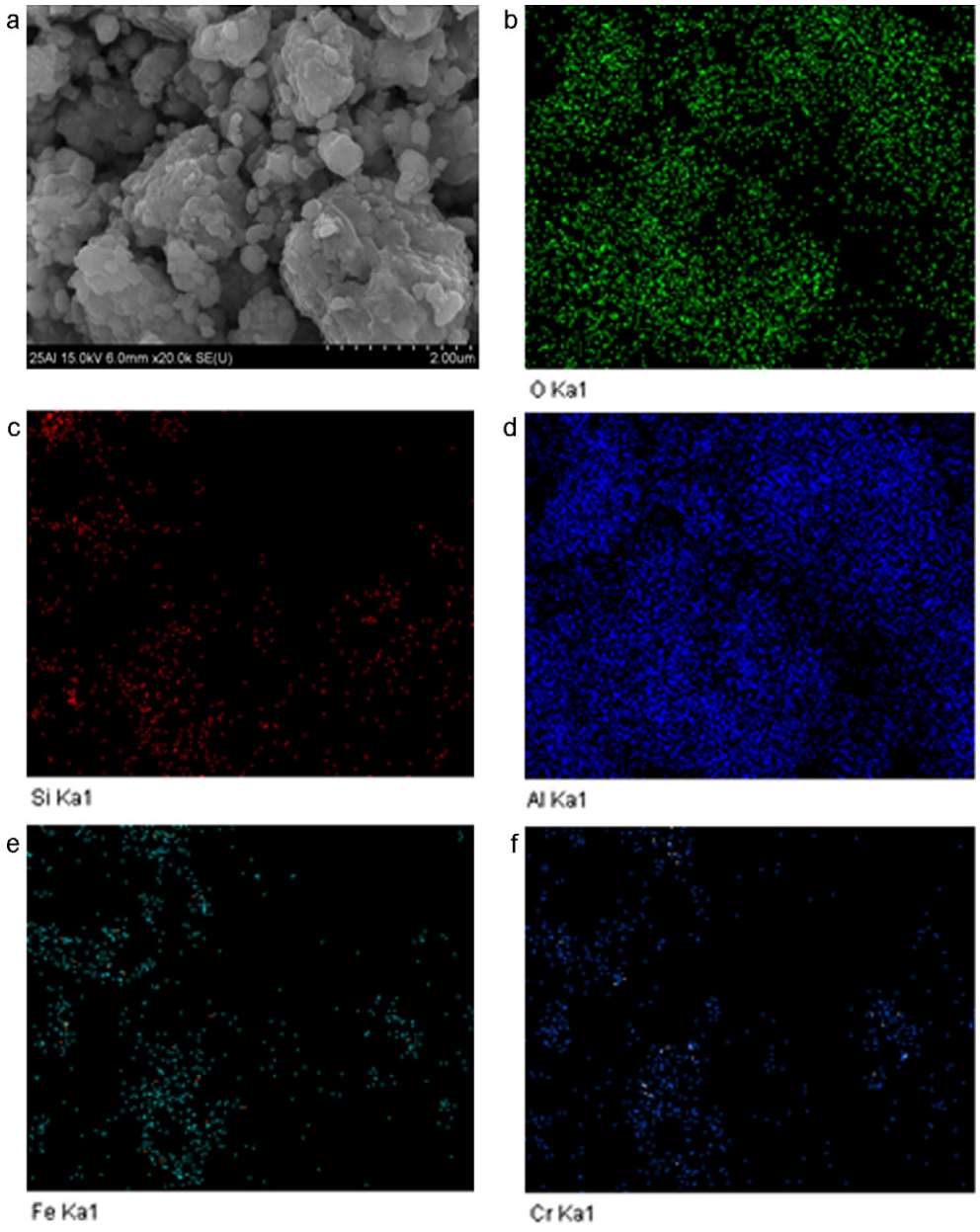

Fig. 2. FE-SEM image of the $5.33Fe_{0.37}Cr_{0.16}Al_{0.4}Si_{0.07}$–$Al_2O_3$ composite and X-ray mapping of O, Al, Si, Fe, and Cr.

used to calculate the crystallite size (L). The average grain sizes of Fe–Cr–Al–Si and Al_2O_3 determined by Suryanarayana's and Norton's formula were about 7 nm and 55 nm, respectively.

Fig. 4 shows the variations in the shrinkage displacement and surface temperature of the graphite die with heating time during the processing of the Fe–Cr–Al–Si and Al_2O_3 system. When an induced current was applied, the specimen experienced thermal expansion, and the shrinkage displacement slowly increased with temperature up to about 900 °C, then increased abruptly at about 1100 °C. The X-ray diffraction pattern of a sample heated to 1050 °C is shown in Fig. 5, where the Fe–Cr–Al–Si alloy and Al_2O_3 were detected. An FE-SEM image of the $5.33Fe_{0.37}Cr_{0.16}Al_{0.4}Si_{0.07}$–$Al_2O_3$ composite is shown in Fig. 6. The figure shows that the structure consisted of nanophases, and pores were not detected. Thus, nearly a full density of nanocomposite was obtained. Fig. 7 shows a plot of $B_r \cos\theta$ versus $\sin\theta$ used to calculate the structure parameters, including the average grain sizes of the Fe–Cr–Al–Si alloy and Al_2O_3. The grain sizes of the Fe–Cr–Al–Si alloy and Al_2O_3 obtained from the X-ray data and using Suryanarayana's and Norton's formula were 13 nm and 99 nm, respectively. The average grain sizes of the sintered Fe–Cr–Al–Si alloy and Al_2O_3 were not significantly larger than the initial powders, indicating the absence of significant grain growth during sintering. This retention of the grain size is attributed to the high heating rate and the relatively short exposure of the powders to the high temperature. The role of the current in sintering has been the focus of several attempts to explain the observed enhancement of sintering and the improved characteristics of the products. The role played by the current has been

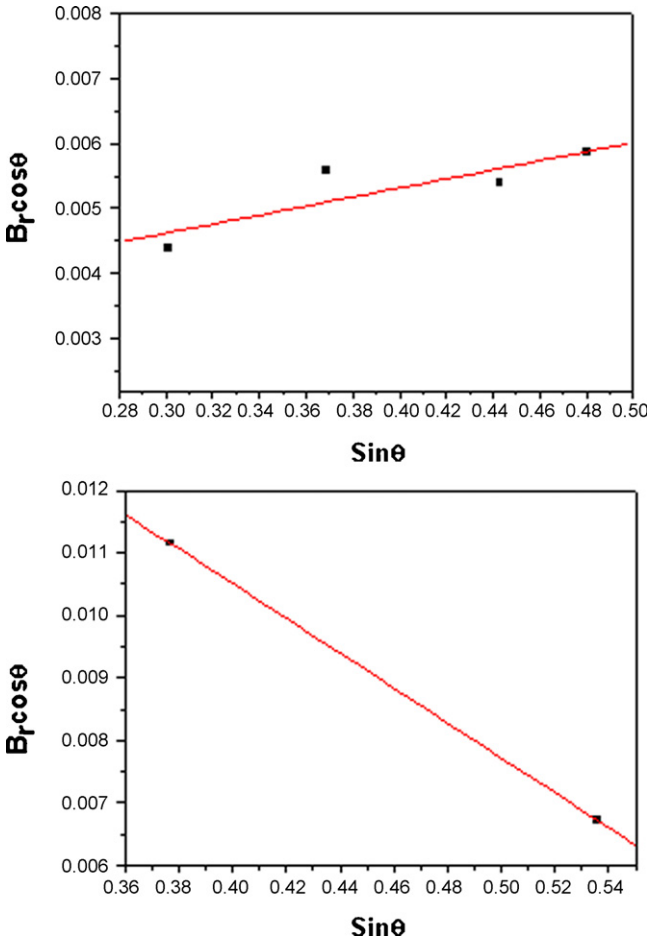

Fig. 3. Plot of $B_r \cos\theta$ vs. $\cos\theta$ of $5.33Fe_{0.37}Cr_{0.16}Al_{0.4}Si_{0.07}$ and Al_2O_3 in the mechanically alloyed powders.

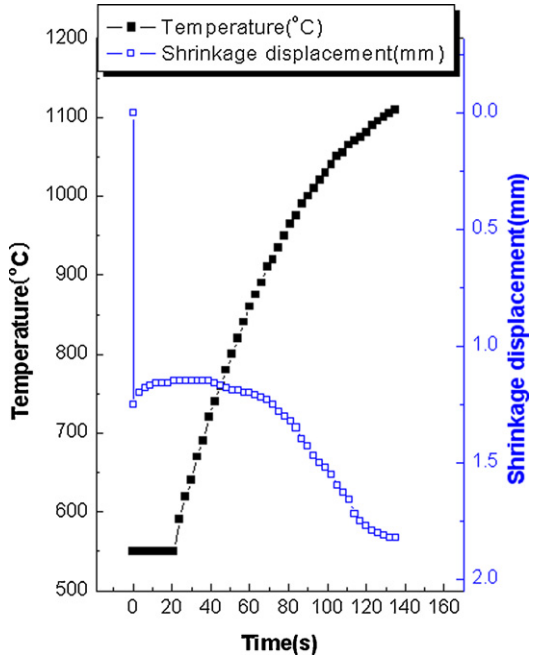

Fig. 4. Variations of the temperature and shrinkage displacement with heating time during high-frequency, induction-heated sintering of $5.33Fe_{0.37}Cr_{0.16}Al_{0.4}Si_{0.07}$–$Al_2O_3$ powders.

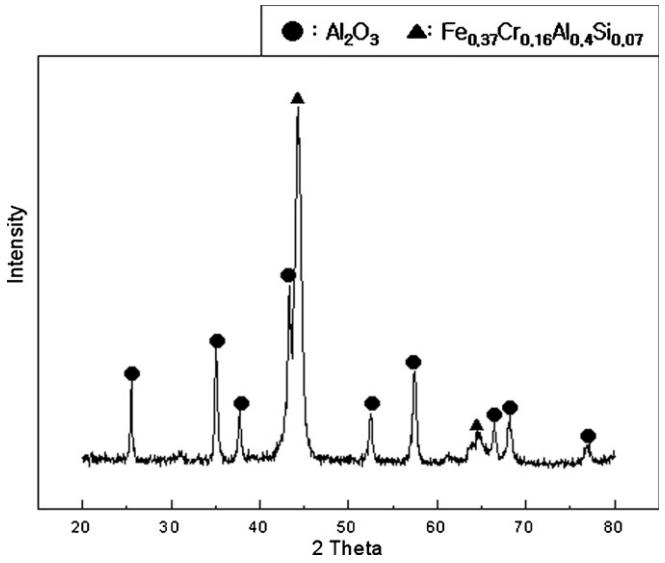

Fig. 5. XRD patterns of the $5.33Fe_{0.37}Cr_{0.16}Al_{0.4}Si_{0.07}$–$Al_2O_3$ composite heated to 1100 °C.

interpreted in terms of the fast heating rate due to Joule heating, the presence of plasma in pores separating powder particles, and the intrinsic contribution of the current to mass transport [14–17].

Vickers hardness measurements were made on polished sections of the $5.33Fe_{0.37}Cr_{0.16}Al_{0.4}Si_{0.07}$–$Al_2O_3$ composite using a 10 kg_f load and a 15 s dwell time. The calculated hardness value of the $5.33Fe_{0.37}Cr_{0.16}Al_{0.4}Si_{0.07}$–$Al_2O_3$ composite was 650 kg/mm^2. This value represents an average of five measurements. This is considered the fracture toughness of $5.33Fe_{0.37}Cr_{0.16}Al_{0.4}Si_{0.07}$–$Al_2O_3$ composite, because cracks were not produced around the indent. The absence of reported hardness and toughness values for the $5.33Fe_{0.37}Cr_{0.16}Al_{0.4}Si_{0.07}$–$Al_2O_3$ composite precludes making direct comparisons to the results obtained in this study. However, the hardness and fracture toughness of Al_2O_3 with a grain size of 4.5 μm were previously reported as 1800 kg/mm^2 and 4 MPa $m^{1/2}$, respectively [18]. The hardness of the

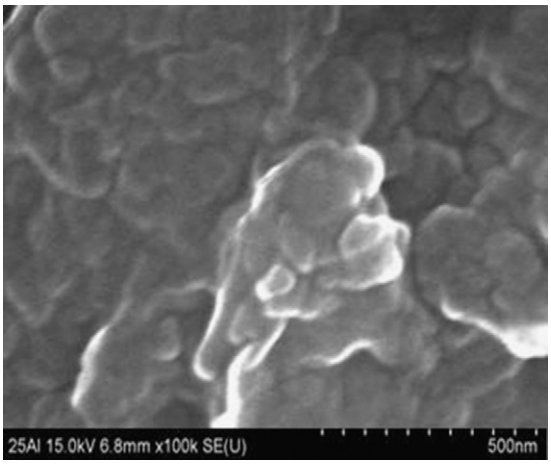

Fig. 6. FE-SEM image of the $5.33Fe_{0.37}Cr_{0.16}Al_{0.4}Si_{0.07}$–$Al_2O_3$ composite heated to 1100 °C.

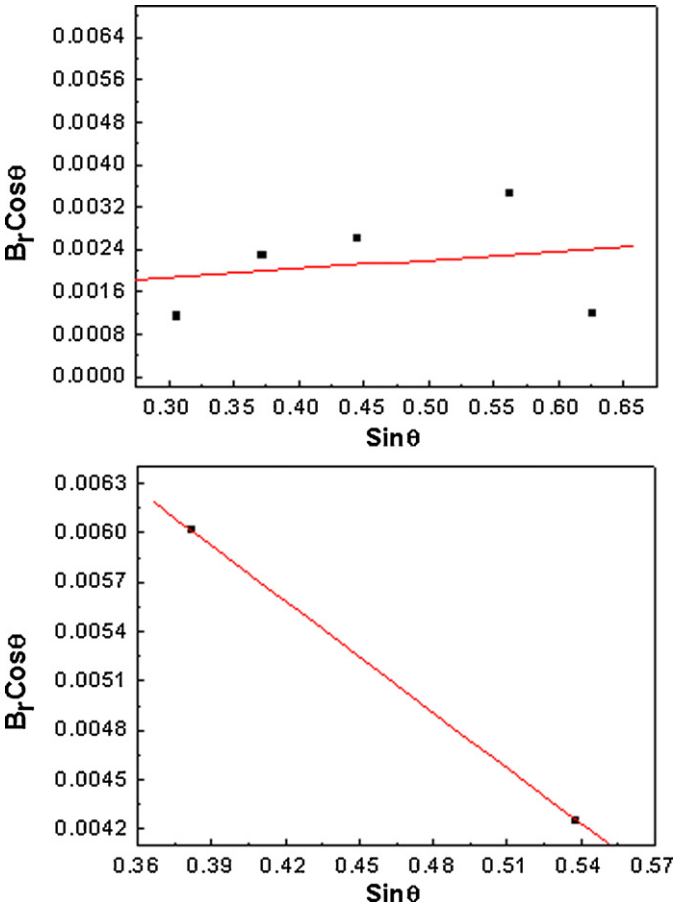

Fig. 7. Plot of $B_r \cos\theta$ vs. $\cos\theta$ of $5.33Fe_{0.37}Cr_{0.16}Al_{0.4}Si_{0.07}$ and Al_2O_3 in the composite sintered at 1100 °C.

$5.33Fe_{0.37}Cr_{0.16}Al_{0.4}Si_{0.07}$–$Al_2O_3$ composite is less than that of monolithic Al_2O_3, but the fracture toughness is greater than that of Al_2O_3 due to the addition of the ductile Fe–Cr–Al–Si alloy.

4. Conclusions

Nanopowders of Fe–Cr–Al–Si and Al_2O_3 were fabricated from Fe_2O_3, Cr, Si, and Al powders by high-energy ball milling. The average grain sizes of the Fe–Cr–Al–Si alloy and Al_2O_3 prepared by HEBM were 7 nm and 55 nm, respectively. Using the high-frequency, induction-activated sintering method, we accomplished densification of nanostructured $5.33Fe_{0.37}Cr_{0.16}Al_{0.4}Si_{0.07}$–$Al_2O_3$ composite from mechanically alloyed powders. Complete densification could be achieved within a processing time of three minutes under an applied pressure of 80 MPa and an induced current. The average grain sizes of the Fe–Cr–Al–Si alloy and Al_2O_3 prepared by HFIHS were about 14 nm and 99 nm, respectively. The average obtained hardness value was 650 kg/mm^2.

Acknowledgements

This work was supported by the New & Renewable Energy R&D Program (2009T00100316) of the Ministry of Knowledge Economy, Republic of Korea.

References

[1] J. Klower, High temperature corrosion behavior of iron aluminides and iron–aluminium–chromium alloys, Materials and Corrosion 47 (1996) 685–694.
[2] P. Kofstad, High Temperature Corrosion, Elsevier Appl. Sci. Publ., London, New York, 1988.
[3] X. Wang, R. Gong, P. Li, L. Liu, W. Chang, Effect of aspect ratio and particle size on the microwave properties of Fe–Cr–Si–Al alloy flakes, Materials Science and Engineering A 466 (2007) 178–182.
[4] V.D.F.C. Lins, M.A. Freitas, E.M.D.P. Silva, Oxidation kinetics of an Fe-31.8Mn-6.09Al-1.60Si–0.40C alloy at temperatures from 600 to 900 °C, Corrosion Science 46 (2004) 1895–1907.
[5] N.R. Park, I.Y. Ko, J.M. Doh, W.Y. Kong, J.K. Yoon, I.J. Shon, Rapid consolidation of nanocrystalline $3Ni–Al_2O_3$ composite from mechanically synthesized powders by high frequency induction heated sintering, Materials Characterization 61 (2010) 277–282.
[6] S. Paris, E. Gaffet, F. Bernard, Z.A. Munir, Spark plasma synthesis from mechanically activated powders: a versatile route for producing dense nanostructured iron aluminides, Scripta Materialia 50 (2004) 691–696.
[7] M.S. El-Eskandarany, Structure and properties of nanocrystalline TiC full-density bulk alloy consolidated from mechanically reacted powders, Journal of Alloys and Compounds 305 (2000) 225–238.
[8] L. Fu, L.H. Cao, Y.S. Fan, Two-step synthesis of nanostructured tungsten carbide–cobalt powders, Scripta Materialia 44 (2001) 1061–1068.
[9] S. Berger, R. Porat, R. Rosen, Nanocrystalline materials: a study of WC-based hard metals, Progress in Materials Science 42 (1997) 311–320.
[10] J. Jung, S. Kang, Sintered (Ti,W)C Carbides, Scripta Materialia 56 (2007) 561–564.
[11] H.C. Kim, I.J. Shon, I.J. Jeong, I.Y. Ko, J.K. Yoon, J.M. Doh, Rapid sintering of ultra fine WC and WC–Co hard materials by high-frequency induction heated sintering and their mechanical properties, Metals and Materials International 13 (2007) 39–46.
[12] H.C. Kim, I.J. Shon, I.K. Jeong, I.Y. Ko, Rapid sintering of nanocrystalline 8 mol.%Y_2O_3-stabilized ZrO_2 by high-frequency induction heating method, Metals and Materials International 12 (2006) 393–399.
[13] C. Suryanarayana, M. Grant Norton, X-ray Diffraction a Practical Approach, P. 213, Plenum Press, 1998.
[14] Z. Shen, M. Johnsson, Z. Zhao, M. Nygren, Spark plasma sintering of alumina, Journal of American Ceramic Society 85 (2002) 1921–1927.
[15] J.E. Garay, U. Anselmi-Tamburini, Z.A. Munir, S.C. Glade, P. Asoka-Kumar, Electric current enhanced defect mobility in Ni_3Ti, Applied Physics Letters 85 (2004) 573–575.
[16] J.R. Friedman, J.E. Garay, U. Anselmi-Tamburini, Z.A. Munir, Modified interfacial reactions in Ag–Zn multilayers under the influence of high DC currents, Intermetallics 12 (2004) 589–597.
[17] J.E. Garay, U. Anselmi-Tamburini, Z.A. Munir, Enhanced growth of intermetallic phases in the Ni–Ti system by current effects, Acta Materialia 51 (2003) 4487–4495.
[18] N.R. Mohamed, Y. Aihua, B.S. Bal, J.P. Garino, M.D. Ries, Ceramics for prosthetic hip and knee joint replacement, Journal of American Ceramic Society 90 (2007) 1965–1988.